Received 28 October 2018; revised 27 March 2019 and 3 July 2019; accepted 6 July 2019. Date of publication 12 July 2019; date of current version 18 September 2019.

Digital Object Identifier 10.1109/JPETS.2019.2928013

A Generic EMT-Type Model for Wind Parks With Permanent Magnet Synchronous Generator Full Size Converter Wind Turbines

U. KARAAGAC[1], J. MAHSEREDJIAN[2], R. GAGNON[3], H. GRAS[2], H. SAAD[4], L. CAI[5], I. KOCAR[2], A. HADDADI[2], E. FARANTATOS[6], S. BU[1], K. W. CHAN[1], AND L. WANG[7]

[1]Department of Electrical Engineering, The Hong Kong Polytechnic University, Hong Kong
[2]Polytechnique Montréal, Montréal, QC H3C 3A7, Canada
[3]IREQ (Hydro-Quebec), Varennes, QC J3X 1S1, Canada
[4]Réseau de Transport d'Electricité, 92800 Paris, France
[5]Department of Electrical Engineering, University of Rostock, 18059 Rostock, Germany
[6]Electric Power Research Institute (EPRI), Palo Alto, CA 94303, USA
[7]Department of Electrical Engineering, University of British Columbia, Kelowna, BC V1V 1V7, Canada
CORRESPONDING AUTHOR: J. MAHSEREDJIAN (jean.mahseredjian@polymtl.ca)

ABSTRACT Utilities are under considerable pressure to increase the share of wind energy resources in their generation fleet. With the increasing share of wind energy resources, the dynamic behavior of power systems will change considerably due to fundamental differences in technologies used for wind and conventional generators. There is a very little standardization in the ways to model wind turbines (WTs) and wind parks (WPs) in sharp contrast to conventional power plants. Hence, there is an international interest to deliver generic models (i.e. standardized and publicly available) for WTs and WPs that are able to capture all performance aspects as good as manufacturer-specific models. This paper presents an electromagnetic transient (EMT) simulation model for full-size converter (FSC) WT-based WPs that can be used for stability analysis and interconnection studies. The considered topology uses a permanent magnet synchronous generator. Although the collector grid and the FSC WTs are represented with their aggregated models, the overall control structure of the WP is preserved. FSC WT and WP control systems include the non-linearities, and necessary transient and protection functions to simulate the accurate transient behavior of WPs.

INDEX TERMS Electromagnetic transient program, full size converter, wind park, wind turbine.

I. INTRODUCTION

WITH recent advances in wind turbine (WT) technology, the wind power penetration levels increase as well as the sizes of WTs and wind parks (WPs). The large scale WPs employ variable speed wind turbines (VSWTs) in order to increase energy capture, reduce drive train stresses and comply with grid code requirements [1]. Full size converter (FSC) and Doubly-fed induction generator (DFIG) WTs fall into this category.

Interconnecting a large-scale WP into a bulk power system has become a more important issue due to its significant impact on power system transient behavior. Failure to perform proper interconnection studies could lead to not only non-optimal designs and operations of WPs, but also severe power system operation and even stability problems. Manufacturer-specific models of WPs are normally favored for interconnection studies due to their fidelity. However, these WP models are typically delivered as black box models. Such models do not enable analysis of internal systems for detection of potential performance issues. Utilities and project developers require accurate generic WP models to perform preliminary grid integration studies before an actual design is selected. Accurate generic WP models will also enable researchers to identify WP grid integration issues and propose proper countermeasures.

Most of existing generic VSWT based WP models [2]–[6] have been developed for system stability studies and they are phasor domain (positive sequence) models. The DFIG based

WP models in [2], [3] are obtained by scaling up a WT model to desired power without taking the WP controller (WPC) into account. It should be noted that this approach is widely used in generic WP models [7]. The WP voltage/reactive power control scheme in [4]–[6] includes a WPC that produces reactive power reference signal for the WTs. Hence, the WT outer control in [4] - [6] uses an automatic reactive power regulator (AQR) for actuating the WT reactive current. On the other hand, using automatic voltage regulator (AVR) for actuating the reactive current provides faster response. Moreover, WPC tuning becomes easier as the system dependency on the short circuit ratio (SCR) is reduced compared to a WP with an AQR at WTs [8]. Therefore, the WP voltage/reactive power control scheme in [4]–[6] is not expected to be common. The generic WP models in [2]–[6] also consider only WTs with coupled control scheme (i.e. no decoupled sequence control). Therefore, they need some refinements, extensions and adaptations.

The phasor domain models of WPs are suitable for transient stability programs (TSPs) and might be adequate for basic power system design studies, such as stability analysis. On the other hand, detailed electromagnetic transient (EMT) models are typically used for equipment design and the assessment of fast electromagnetic transients in arbitrary network topologies with nonlinearities. They are circuit based models and offer the highest accuracy for a wide range of perturbations, including transient stability.

Generic EMT-type simulation models for FSC and DFIG based WPs have been proposed in [9] and [10], respectively. However, the WP and WT control structure in both [9] and [10] are not realistic as the outer loops of WT control (the active power and the voltage/reactive power controls) are moved to the point of interconnection as WPC. The EMT-type simulation models of DFIG based WPs in [11]–[13] have a WP voltage/reactive power control scheme as recommended in [8]. On the other hand, the EMT-type simulation models in [9]–[13] are alike the generic phasor domain models, i.e. they disregard the possible decoupled sequence control (DSC) scheme in WTs.

Ideally, the GSC with traditional coupled sequence control (CSC) scheme is not expected to inject any negative sequence currents to the grid during unbalanced loading conditions or faults. In practice, it injects a very small amount due to the phase shift in low pass measuring filters [14]. Unlike its output currents, the GSC terminal voltages contain negative sequence component during unbalanced loading conditions or faults, and this causes second harmonic oscillations in the GSC active power output as well as the dc bus capacitor voltage. These second harmonic oscillations can be eliminated by adopting a DSC scheme [15]. The DSC scheme in GSC should give the priority to the positive sequence reactive currents designated by the FRT requirement and then use the available converter capacity for the second harmonic oscillation mitigation [16].

As discussed in [17]–[19], lack of negative sequence fault current contribution from the FSC WT with traditional CSC may cause misoperation of protection system during certain unbalanced fault conditions. Although the GSC operating under DSC injects considerable amount of negative sequence currents during unbalanced faults, the recent VDE-AR-N 4120 Technical Connection Rules [20] includes a negative sequence reactive current requirement to further reduce the possibility of protection system misoperation. Hence, the DSC scheme in FSC WTs (if it exists) should be accounted in EMT simulation model.

This paper presents a generic EMT model for FSC WT based WPs that can be used for a wide range of WP integration studies. The collector grid and the FSC WTs are represented with their aggregated models, but the overall control structure of the WP is preserved. The FSC WT and the WP control system models include the non-linearities, necessary transient and protection functions; and allow to simulate the accurate transient behavior of WPs subjected to external power system disturbances.

The first part of this paper briefly presents the WPs with FSC WTs. The EMT model is presented in the second part. The third part presents illustrative simulation examples.

II. VARIABLE SPEED WIND TURBINES

A. WIND TURBINE AERODYNAMICS

The wind turbine extracts kinetic energy from the swept area of the blades. The mechanical power extracted from wind is given by [21]:

$$P_t = (1/2)\,\rho A \upsilon^3 C_p(\lambda, \beta) \tag{1}$$

where ρ is the air density (approximately 1.225 kg/m^3), A is the swept area of the rotor (m^2), υ is upwind free wind speed (m/s) and C_p is the power coefficient. The C_p is usually provided as a set of curves (C_p curves) relating C_p to tip-speed-ratio λ with the blade pitch angle β as a parameter, as shown in Fig. 1 [22]. The tip-speed-ratio is defined as

$$\lambda = (\omega_t R)/\upsilon \tag{2}$$

where ω_t is the WT rotational speed (rad/s) and R is the blade radius (m).

At a specific wind speed and pitch angle, there is a unique WT rotational speed that achieves the maximum power coefficient $C_{P\max}$, hence the maximum mechanical power as shown in Fig. 1.

The mathematical model of WT aerodynamics is shown in Fig. 2. In this modeling approach, the C_p curves of the WT are fitted with high order polynomials on λ and β as

$$C_p(\lambda, \beta) = \sum_{i=1}^{n}\sum_{j=1}^{n} \alpha_{ij}\lambda^i\beta^j \tag{3}$$

The alternative representation of WT aerodynamics includes using C_p- matrix in which the C_p coefficients are stored in a large matrix. This approach represents the WT aerodynamics more accurately and its usage in WT simulation models is recommended in IEC 61400-27 [23]. Replacing the implemented polynomial representation with

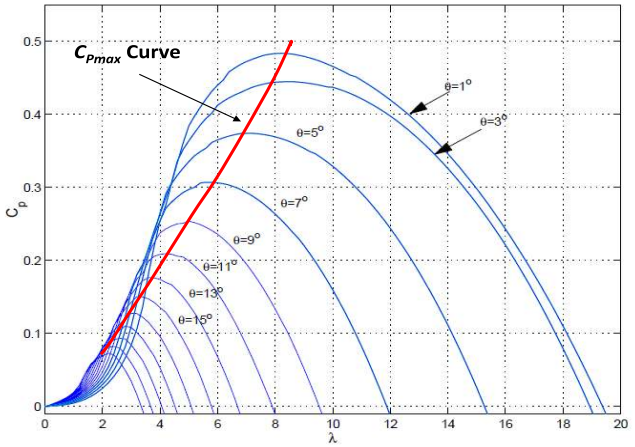

FIGURE 1. Wind Power C_p curves.

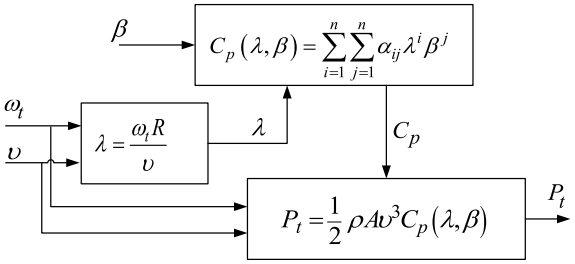

FIGURE 2. Wind turbine aerodynamics model.

C_p- matrix might be essential when the EMT-type simulation tool is used to simulate long term dynamics. On the other hand, depending on the simulated phenomenon, the WT aerodynamics might have negligible impact on simulation results and can be totally disregarded in EMT-type simulations in order to reduce the simulation cost.

B. MECHANICAL SYSTEM

The mechanical system is constituted by the blades linked to the hub coupled to the slow shaft. The shaft is linked to the gearbox which multiplies the rotational speed of the fast shaft connected to the generator. Although the mechanical representation of the entire WT is complex, representing the fundamental resonance frequency of the drive train using its two mass model is sufficient as the other resonance frequencies are much higher and their magnitudes are lower [24].

C. CONTROL OF VARIABLE SPEED WIND TURBINES

The control of VSWT calculates the generator power output and the pitch angle in order to achieve extracting the maximum energy from the wind and keeping the WT in safe operating mode. The WT remains shut down when the wind speed is too low for energy production (i.e. below cut-in speed υ_{cut-in}). When the wind speed is above υ_{cut-in} and below rated speed υ_{rated}, the pitch angle is kept at zero ($\beta = 0^0$) and the power reference of the WT generator is produced by the MPPT (maximum power point tracking) function to achieve optimal operation. The conventional method is to calculate

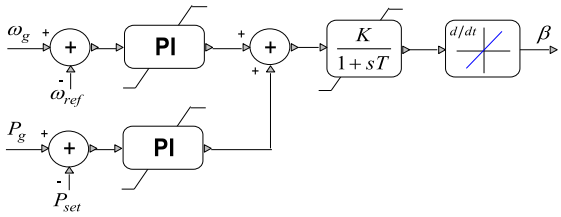

FIGURE 3. Schematic diagram of pitch control.

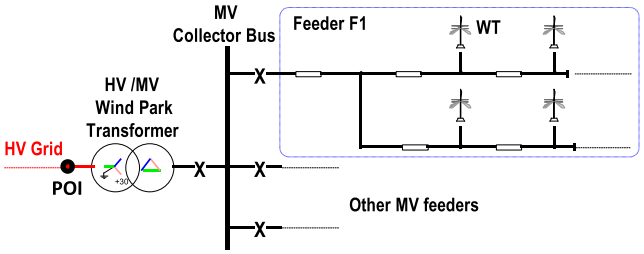

FIGURE 4. Simplified single-line diagram of a typical wind park.

the power reference using a cubic function of the turbine angular speed.

$$P_{ref} = K_{opt}\ \omega_t^3 \tag{4}$$

where

$$K_{opt} = (1/2)\, C_{p-\max}\ \rho\ A\ \left(R\ /\lambda_{opt}\right)^3 \tag{5}$$

The relation between the available aerodynamic power and wind speed is cubic at only low wind speeds in modern WTs. IEC 61400-27 suggests using cubic relation up to the wind speed that outputs 0.3 per-unit power and linear relation after. Reader should refer to [23] for details.

When the wind speed is above υ_{rated}, the pitch angle is increased by the pitch controller (see Fig. 3) in order to limit the mechanical power extracted from the wind and reduce the mechanical loads on the drive train. It should be noted that the pitch controller should ensure zero pitch angle ($\beta = 0^0$) for the wind speeds below υ_{rated} [25]. Above cut-off speed $\upsilon_{cut-off}$, the WT is shut down. IEC 61400-27 suggests a more advanced pitch control with cross-coupling and modification of the reference values ω_g and P_g to avoid unintended operating points following grid faults.

The power pitch controller can be improved further by the power recovery algorithm (after FRT) and frequency control scheme described in IEC 61400-27.

III. WIND PARKS WITH VARIABLE SPEED WIND TURBINES

The power produced by the WTs is transmitted to the high voltage (HV) transmission grid through the medium voltage (MV) collector grid and WP transformer as shown in Fig. 4. Usually, the WP transformer has an on-load-tap-changer to keep the MV collector bus voltage around its nominal value. The active power at point of interconnection (POI) depends on wind conditions at each WT inside the WP and

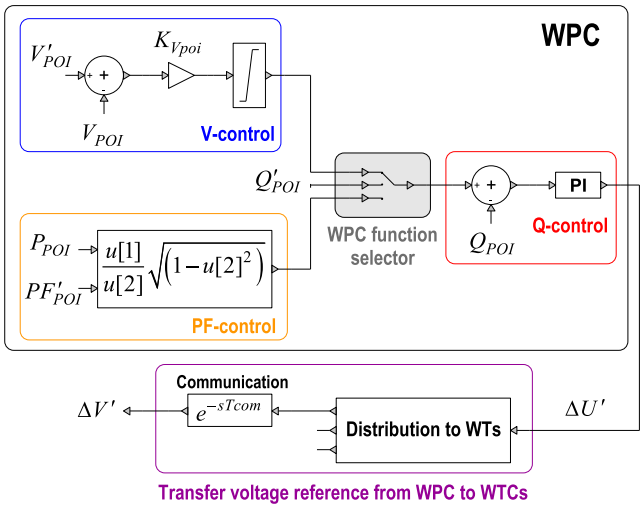

FIGURE 5. **Wind park controller.**

is determined by the MPPT function (see (4)) when the wind speed is between υ_{cut-in} and υ_{rated}. On the other hand, the reactive power at POI is controlled by a central WPC which is located at the WP substation.

The voltage at POI (V_{POI}) is controlled with a proportional controller (V-control). Generally, the proportional gain of this controller and the reference value for the voltage at POI (V'_{POI}) are defined by the transmission system operator [8]. The proportional voltage regulator gain of WPC can be defined as

$$K_{Vpoi} = \Delta Q_{POI} / \Delta V_{POI} \tag{6}$$

When the WTs are equipped with AQR for actuating the reactive currents, the reactive power reference values calculated by the WPC voltage regulator are sent to the WTs.

When the WTs are equipped with AVR for actuating the reactive currents, the WPC also contains a proportional-integral (PI) reactive power regulator which modifies the wind turbine control (WTC) reference voltage values (V') through a proportional-integral (PI) reactive power regulator as illustrated in Fig. 5. This figure also illustrates the WPC control options that regulate reactive power at POI (Q-control) and power factor control (PF-control). T_{com} in Fig. 5 is the communication delay.

When a severe voltage sag occurs at POI due to a fault, the PI regulator output ($\Delta U'$) is kept constant by blocking its input (i.e. zero is applied instead of ($Q'_{POI} - Q_{POI}$) as input signal). This is to avoid overvoltage after fault removal.

In this section and hereinafter, all variables are in pu (unless the opposite is stated) and primed variables are used to denote reference values from controllers.

IV. FULL SIZE CONVERTER WIND TURBINES

A FSC WT may or may not have a gearbox. A wide range of electrical generators such as asynchronous, synchronous and permanent magnet can be used. The WT power is transferred

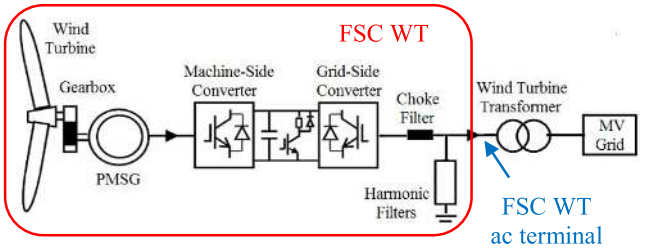

FIGURE 6. **Schematic diagram of FSC WT.**

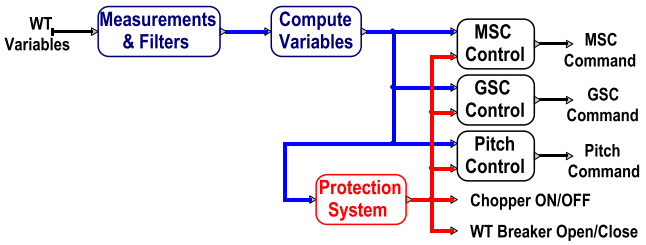

FIGURE 7. **Simplified diagram, FSC WT control and protection system.**

through an ac-dc-ac converter system, and the dynamics of the electrical generator are isolated from the grid [26].

The considered topology in this paper is shown in Fig. 6. It uses a permanent magnet synchronous generator (PMSG) and the ac-dc-ac converter system consisting of two pulse-width modulated (PWM) voltage source converters (VSCs): machine-side converter (MSC) and grid-side converter (GSC). The dc resistive chopper is used for the dc bus overvoltage protection. The line inductor (choke filter) and ac harmonic filters are used at the GSC to improve power quality.

Fig. 7 depicts the simplified diagram of FSC WT control and protection systems. The sampled signals are converted to per unit and filtered with low-pass filters with the ''Measurements & Filters'' block. The variables used by the FSC WT control and protection system are calculated at ''Compute Variables'' block. The ''Protection System'' block contains dc resistive chopper control, MSC and GSC overcurrent protections, low voltage and overvoltage relays, cut-in and cut-off speed relays. The ''Pitch Control'' block (see Fig. 3) limits the mechanical power extracted from wind by increasing the pitch angle when the wind speed is above its rated value.

As shown in Fig. 8, WT converters are controlled using vector control. The MSC and GSC signals are transferred to the flux and voltage reference frames, respectively. Both converters are controlled by a two-level controller. The slow outer control calculates the reference dq-frame currents. The fast inner (current) control produces the converter ac voltage reference.

A. MACHINE SIDE CONVERTER CONTROL

The q- and d-axis currents of MSC (i_{qm} and i_{dm} in Fig. 8) are used to control the active and reactive power outputs of

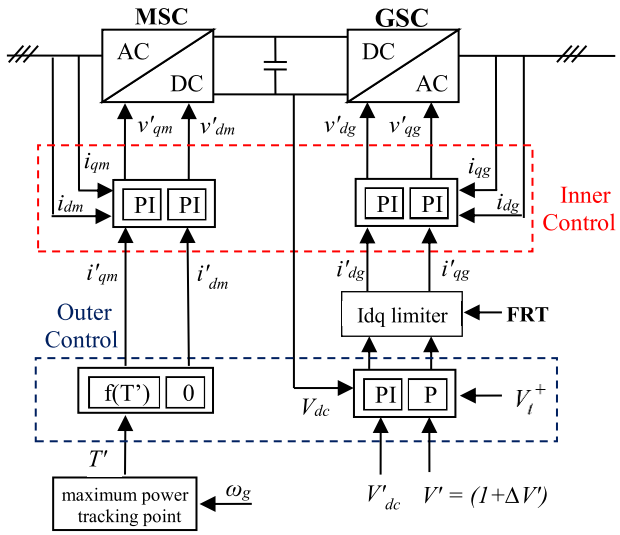

FIGURE 8. Schematic diagram of FSC WT control.

the PMSG, respectively. The q-axis current reference ($f(T')$ in Fig. 8) is given by

$$i'_{qm} = T'/\lambda_m \tag{7}$$

where λ_m is the constant flux generated by the permanent magnet and $T' = K_{opt}\ \omega_t^2$ is the reference for PMSG electromagnetic torque given by the MPPT control.

The d-axis current reference is set to zero ($i'_{dm} = 0$) to achieve unity power factor.

The MSC inner control loop is designed based on internal model control (IMC) method [27]. This method enables calculation of dq-frame proportional integral (PI) controller parameters (gain and integration time constant) using certain machine parameters and the desired closed-loop bandwidth. This method simplifies the controller design procedure and eliminates (or reduces) the need for trial-and-error.

The PMSG stator voltages are found from

$$v_{dm} = -R_s i_{dm} - L_d\,(d\ i_{dm}/dt) + \omega_g L_q i_{qm} \tag{8}$$

$$v_{qm} = -R_s i_{qm} - L_q\,(d\ i_{qm}/dt) + \omega_g\,(L_d i_{dm} + \lambda_m) \tag{9}$$

where R_s is the armature resistance, L_d and L_q are the d- and q-axis inductances of PMSG.

The i_{dm} and i_{qm} errors are processed by the PI controller to give v_{dm} and v_{qm}, respectively. To ensure good tracking, feed-forward compensating terms $\omega_g L_q i_{qm}$ in (8) and $\omega_g\,(L_d i_{dm} + \lambda_m)$ in (9) are added. The converter reference voltages become

$$v'_{dm} = -\left(k_p^d + k_i^d/s\right)\left(i'_{dm} - i_{dm}\right) + \omega_g L_q i_{qm} \tag{10}$$

$$v'_{qm} = -\left(k_p^q + k_i^q/s\right)\left(i'_{qm} - i_{qm}\right) + \omega_g\,(L_d i_{dm} + \lambda_m) \tag{11}$$

Using IMC, the PI controller parameters are found as

$$k_p^d = \alpha_c L_d, \quad k_p^q = \alpha_c L_q,\ k_i^d = k_i^q = \alpha_c R_s \tag{12}$$

where α_c is the bandwidth. The relationship between the bandwidth and the rise time (10%–90%) is $\alpha_c = \ln(9)/t_{rise}$.

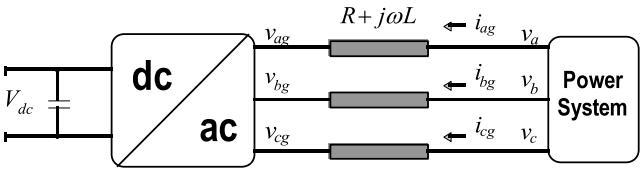

FIGURE 9. GSC arrangement.

B. GRID SIDE CONVERTER CONTROL

The GSC function is maintaining the dc bus voltage V_{dc} at its nominal value and also controlling its positive sequence ac terminal voltage (V_t^+) when equipped with AVR (see Fig. 8). The q-axis reference current is calculated by the proportional outer voltage control.

$$i'_{qg} = K_V\left(V' - V_t^+\right) \tag{13}$$

where K_V is the voltage regulator gain. The reference for FSC positive sequence voltage ($V' = 1 + \Delta V'$) is calculated by the WPC (see Fig. 5).

When AQR is used to control the GSC reactive current output, q-axis reference current is calculated by a PI reactive power regulator.

$$i'_{qg} = \left(K_p^Q + K_i^Q/s\right)\left(Q'_{WT} - Q_{WT}\right) \tag{14}$$

where K_p^Q and K_i^Q are the reactive power regulator parameters, Q_{WT} is the reactive power output of the FSC WT (including harmonic filters) and Q'_{WT} is the reference is calculated by the WPC. Reader should refer to [8] for details.

The d-axis reference current is calculated by the proportional outer dc voltage control. It is a PI controller tuned based on inertia emulation, with

$$k_p = \omega_0^2\,(2H_{Cdc}), \quad k_i = 2\xi\omega_0\,(2H_{Cdc}) \tag{15}$$

where ω_0 is the natural frequency of the closed loop system and ξ is the damping factor. $H_{Cdc} = (E_{Cdc}/S_{wt})$ is the static moment of inertia, E_{Cdc} is the stored energy in dc bus capacitor (in Joules) and S_{wt} is the WT rated power (in VA).

The schematic of the GSC connected to the power system is shown in Fig. 9. $Z = R + j\omega L$ represents the total impedance between the GSC and external HV system Thevenin source, i.e.

$$Z = Z_{HV-grid} + Z_{TR-WP} + Z_{CG} + Z_{TR-WT} + Z_{choke} \tag{16}$$

where $Z_{HV-grid}$ is the external HV system Thevenin impedance, Z_{TR-WP} is the wind park transformer impedance, Z_{CG} is the equivalent MV collector grid series impedance, Z_{TR-WT} is the aggregated wind turbine transformer impedance and Z_{Choke} is aggregated wind turbine choke filter impedance.

The voltage equation is given by (bold characters are used for vectors and matrices)

$$\mathbf{v_{abc}} = \mathbf{R}\ \mathbf{i_{gabc}} + \mathbf{L}\left(d\ \mathbf{i_{gabc}}/dt\right) + \mathbf{v_{gabc}} \tag{17}$$

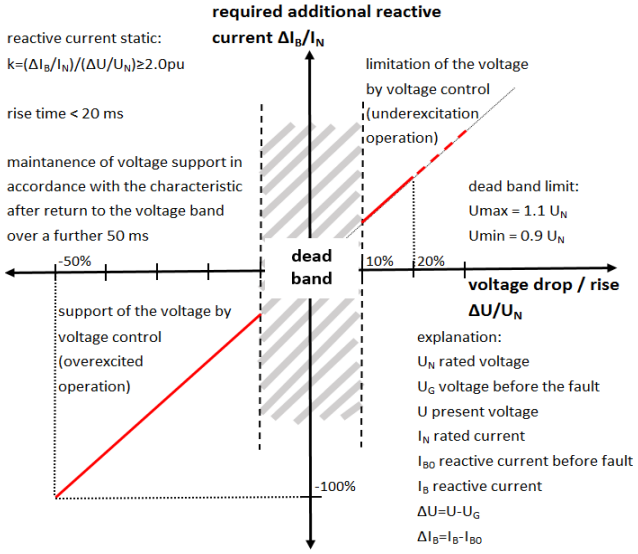

FIGURE 10. **Wind turbine reactive output current during voltage disturbances [28].**

The link between GSC output current and voltage can be described by a transfer function

$$G(s) = 1/(R + sL) \tag{18}$$

Using the IMC method, the PI controller parameters of the inner current control loop are found as

$$k_p = \alpha_c L \ , \quad k_i = \alpha_c R \tag{19}$$

Similar to MSC, the feed-forward compensating terms $\left(\omega L_{choke} i_{qg} + v_{dt}\right)$ and $\left(-\omega L_{choke} i_{dg} + v_{qt}\right)$ are added to the d- and q-axis voltages calculated by the PI regulators, respectively. L_{choke} is the inductance of the aggregated wind turbine choke filter, v_{dt} and v_{qt} are the FSC terminal voltages in dq reference frame. The FSC terminal is illustrated in Fig. 6.

C. FAULT-RIDE-THROUGH FUNCTION

During normal operation, the controller gives priority to the active currents, i.e.

$$\begin{aligned} i'_{dg} &< I_{dg}^{\lim} \\ i'_{qg} &< I_{qg}^{\lim} = \sqrt{\left(I_g^{\lim}\right)^2 - \left(i'_{dg}\right)^2} \end{aligned} \tag{20}$$

where $I_{dg}^{\lim}$, $I_{qg}^{\lim}$ and $I_g^{\lim}$ are the limits for d-axis, q-axis and total GSC currents, respectively.

The grid code requirements, such as [28], include the WT transient response against severe voltage disturbances (see Fig. 10). To comply with this requirement, an FRT function is traditionally added to the WTC. The FRT function is activated when the voltage $|1 - V_{MV}^{+}|$ exceeds the pre-defined value V_{FRT-ON} and deactivated when $|1 - V_{MV}^{+}|$ reduces below the pre-defined value $V_{FRT-OFF}$ after a pre-specified release time t_{FRT}. In the presented generic model, $V_{FRT-ON} = 0.1$ pu, $V_{FRT-OFF} = 0.075$ pu and $t_{FRT} = 250$ ms. V_{MV}^{+} is the WT transformer MV terminal positive sequence voltage and it is estimated in "Compute Variables" block (see Fig. 7) using the WT transformer parameters and measured FSC WT ac terminal voltages and currents. During FRT operation, the GSC controller gives priority to reactive current by reversing the d- and q-axis current limits given in (20). The limits for d-axis, q-axis and total GSC currents might be also different during FRT operation. Reader should refer to [16] for details.

Due to AVR usage, the voltage control is continuous even inside the dead-band region shown in Fig. 10. On the other hand, the reactive current output is limited with the available reserve on GSC as the priority is given to the active currents (see (20)).

When AQR is used to for controlling reactive current output of GSC, it is switched to AVR during FRT operation to achieve the desired reactive current injection from the GSC. The voltage reference of the AVR is set to the pre-disturbance voltage value and AQR input is blocked. Reader should refer [23] for details.

Depending on the manufacturer and grid code requirements, it is possible to have different control schemes. To imitate the accurate fault behavior of the WT, more detailed limitation functions can be used (when available), such as reactive power or reactive current as function of voltage table as described in IEC 61400-27.

D. GSC DECOUPLED SEQUENCE CONTROL

DSC scheme enables controlling converter output currents independently as active and reactive components for both positive and negative sequences. The DSC objective is typically elimination of second harmonic pulsations in the active power output of FSC WT during unbalanced loading conditions or faults. The other objective can be injecting desired level negative sequence reactive currents during unbalanced faults [20].

1) TRADITIONAL DSC (DSC1)

The instantaneous active and reactive powers during unbalanced grid conditions can be written as [15]

$$\begin{aligned} p &= P_0 + P_{C2}\cos(2\omega t) + P_{S2}\sin(2\omega t) \\ q &= Q_0 + Q_{C2}\cos(2\omega t) + Q_{S2}\sin(2\omega t) \end{aligned} \tag{21}$$

where P_0 and Q_0 are the average values of the instantaneous active and reactive powers respectively, whereas P_{C2}, P_{S2}, Q_{C2} and Q_{S2} represent the magnitudes of the second harmonic oscillating terms in these instantaneous powers.

With DSC usage, four of the six power magnitudes in (21) can be controlled for a given grid voltage conditions. As the oscillating terms (P_{C2} and P_{S2}) in active power cause oscillations in dc bus voltage V_{dc}, the GSC current references ($i_{dg}^{+\prime}$, $i_{qg}^{+\prime}$, $i_{dg}^{-\prime}$ and $i_{qg}^{-\prime}$) are calculated to cancel out these terms (i.e. $P_{C2} = P_{S2} = 0$).

The GSC DSC implementation in [16] keeps the outer control and Idq limiter shown in Fig. 8, to calculate i'_{dg}, i'_{qg}, $I_{dg}^{\lim}$ and $I_{qg}^{\lim}$. These values are used to calculate the GSC

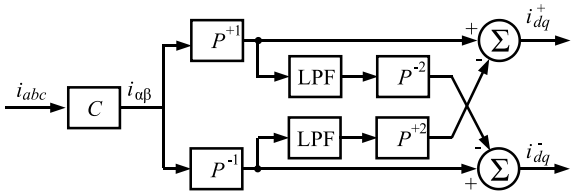

FIGURE 11. Sequence extraction using decoupling method.

current references $i^{+\prime}_{dg}$, $i^{+\prime}_{qg}$, $i^{-\prime}_{dg}$ and $i^{-\prime}_{qg}$ for the DSC. As the positive sequence reactive current injection during faults is defined by the grid code (see Fig. 10), the GSC current reference calculation in [15] is modified as

$$\begin{bmatrix} i^{+\prime}_{qg} \\ i^{+\prime}_{dg} \\ i^{-\prime}_{qg} \\ i^{-\prime}_{dg} \end{bmatrix} = \begin{bmatrix} 1 & 0 & 0 & 0 \\ v^{+}_{qg} & v^{+}_{dg} & v^{-}_{qg} & v^{-}_{dg} \\ v^{-}_{qg} & v^{-}_{dg} & v^{+}_{qg} & v^{+}_{dg} \\ -v^{-}_{dg} & v^{-}_{qg} & v^{+}_{dg} & -v^{+}_{qg} \end{bmatrix}^{-1} \begin{bmatrix} i'_{qg} \\ P_0 \\ P_{C2} \\ P_{S2} \end{bmatrix} \tag{22}$$

where P_0 is approximated by $P_0 = V^{+}_{t}\, i'_{dg}$.

The calculated reference values in (22) are revised considering the converter limits $I^{\lim}_{dg}$ and $I^{\lim}_{qg}$. For example when $\left(i^{+\prime}_{qg} + i^{-\prime}_{qg}\right) > I^{\lim}_{qg}$, the q-axis current references are revised as below

$$\begin{aligned} i^{+\prime\prime}_{qg} &= i^{+\prime}_{qg}\left[I^{\lim}_{qg} / \left(i^{+\prime}_{qg} + i^{-\prime}_{qg}\right)\right] \\ i^{-\prime\prime}_{qg} &= i^{-\prime}_{qg}\left[I^{\lim}_{qg} / \left(i^{+\prime}_{qg} + i^{-\prime}_{qg}\right)\right] \end{aligned} \tag{23}$$

where $i^{+\prime\prime}_{qg}$ and $i^{-\prime\prime}_{qg}$ are the revised reference values for GSC q-axis positive and negative sequence currents, respectively.

The revised GSC d-axis positive and negative sequence current references $i^{+\prime\prime}_{dg}$ and $i^{-\prime\prime}_{dg}$ can be obtained with the same approach using $I^{\lim}_{dg}$. It should be emphasized here that, during faults, the priority is to provide i^{+}_{qg} specified by the grid code. The remaining reserve in GSC is used for eliminating P_{C2} and P_{S2}. Hence, its performance reduces with decreasing electrical distance between the WP and the unbalanced fault location.

As i^{+}_{dg}, i^{+}_{qg}, i^{-}_{dg} and i^{-}_{qg} are controlled, the DSC contains four PI regulators and requires sequence extraction for GSC currents and voltages. Numerous methods have been proposed for sequence extraction in the literature. The implementation in [16] uses the sequence decoupling method [30] shown in Fig. 11. In this method, a combination of a low-pass filter (LPF) and double-line frequency Park transformation (P^{-2} and P^{+2}) is used to produce the oscillating signal, which is then subtracted. The blocks C and P represent the Clarke and Park transformation matrices, and the superscripts ± 1 and ± 2 correspond to direct and inverse transformation at line frequency and double-line frequency, respectively.

In [16], the feed-forward compensating terms ($\omega L_{choke} i_{qg} + v_{dt}$) and ($-\omega L_{choke} i_{dg} + v_{qt}$) are kept in coupled form and added to the PI regulator outputs in stationary $\alpha\beta$-frame.

The GSC DSC implementation for AQR usage can be found in [15]. During FRT operation, it is switched to the DSC scheme presented in this section to achieve the desired positive sequence reactive current injection from the GSC. The voltage reference of the AVR is set to the pre-disturbance voltage value and AQR input is blocked to prevent overvoltage after fault removal.

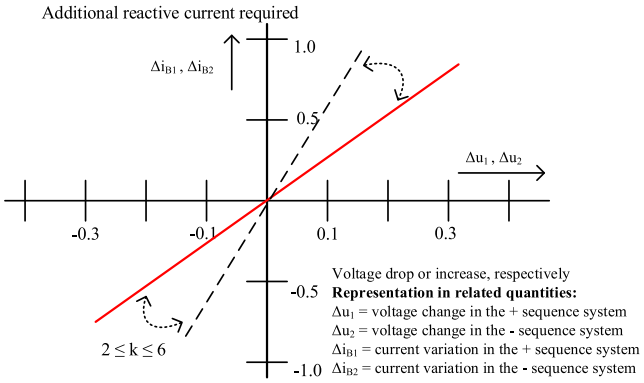

FIGURE 12. Wind turbine reactive output current during voltage disturbances [20].

2) DSC COMPLIANT WITH VDE-AR-N 4120 (DSC2)

In the recent VDE-AR-N 4120 Technical Connection Rules, there is also a required additional negative sequence reactive current as a function of the voltage change in the negative sequence system as shown in Fig. 12. The goal is to reduce the negative sequence voltage by consuming negative sequence reactive power. During FRT operation, the negative sequence reactive current is proportional to the voltage

$$i^{-\prime}_{qg} = K_{V-neg} V^{-}_{t} \tag{24}$$

where K_{neg} is the proportional gain between negative sequence voltage and reactive current, that varies between 2 and 6 as given in Fig. 12.

The positive sequence reactive current reference is calculated by the outer control proportional voltage regulator (see (13)). The reactive current references have to be revised using (23) when $\left(i^{+\prime}_{qg} + i^{-\prime}_{qg}\right) > I^{\lim}_{qg}$.

The positive sequence active current reference is generated by the dc bus voltage regulator ($i^{+\prime}_{dg} = i'_{dg}$) and $i^{-\prime}_{dg} = 0$ as there is no active power exchange on negative sequence.

During normal operation, the controller gives priority to the positive sequence active current (see (20)). On the other hand, during FRT operation, the GSC controller gives priority to reactive current by reversing the d- and q-axis current limits given in (20).

As there is no dead-band region in VDE-AR-N 4120, AVR usage is essential to control GSC reactive current output.

V. IMPLEMENTATION

The complete design of a WT model in a typical EMT software package (EMTP [31] is used in this paper) is based on hierarchical (subnetworks containing subnetworks) blocks with masking. It consists of the aggregated FSC WT, the aggregated LV/MV WT transformer, the equivalent PI

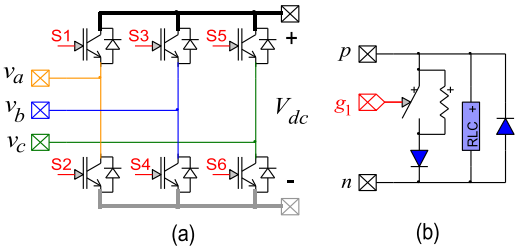

FIGURE 13. **(a) Two level VSC circuit. (b) IGBT valve model.**

circuit of the MV collector grid and the MV/HV WP transformer.

The aggregated and single unit model per unit parameters are same for both FSC WT and WT transformer when the base power for the aggregated unit is selected as

$$S_{agg} = N\ S_{single} \tag{25}$$

where S_{single} is the single unit base power, N is the number of units in aggregation.

The FSC WT control offers both AVR and AQR usage at GSC. When AQR usage at GSC is selected, the reactive power reference for the aggregated WT model is produced by the proportional voltage control of WPC. When AVR usage at GSC is selected, the reactive power regulator of the WPC adjusts the voltage reference value of the aggregated WT model (see Fig. 5 and Fig. 8). For AVR usage (at GSC) selection, the WPC offers POI reactive power and POI power factor control options (Q-control and PF-control, respectively) in addition to the POI voltage control option as shown in Fig. 5. In addition, the user can deactivate WPC. In that case, AVR option uses the user defined voltage reference and AQR option uses either user defined reactive power or power factor as suggested in IEC 61400-27.

The FSC WT control offers both DSC options (DSC1 and DSC2) in addition to the traditional CSC option when AVR is selected to control the GSC reactive currents. DSC2 option is not available for AQR selection.

The generic model has two versions: detailed model (DM) and average value model (AVM). In the DM, the WT converters are represented based on the circuit of Fig. 13.a in which the IGBT/diode is modeled by an ideal switch and nonlinear resistors (shown in Fig. 13.b) to mimic the actual behavior accurately. Simulation of such switching circuits with variable topology requires many time consuming mathematical operations and the high frequency PWM signals force small simulation time-step usage. These computational inefficiencies can be eliminated by using AVM, which replicates the average response of converters through simplified functions and controlled sources [32]. AVMs are used for wind generation technologies [33],[34]. AVM of FSC is obtained by replacing the DMs of converters with voltage-controlled sources on the ac side and current-controlled sources on the dc side (see Fig. 14) [35].

The sampled signals are converted to per unit and filtered at ''Measurements & Filters'' block. The sampling

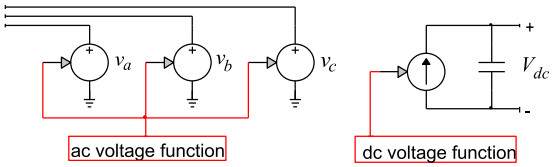

FIGURE 14. **AVM diagram for the two level VSC.**

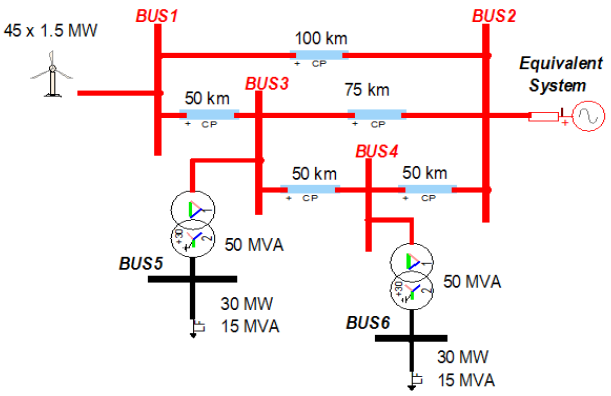

FIGURE 15. **120 kV test system.**

TABLE 1. **Simulation models.**

Model	M1	M2	M3	M4
GSC Control	CSC	DSC1	DSC2	DSC1
Converter Model	DM	DM	DM	AVM

frequencies are set by the user in addition to the PWM frequency (12.5 kHz and 2.5 kHz, respectively, for both MSC and GSC in the presented generic model) and sampling function is deactivated when AVM is used for FSC converters. In the presented generic model, second order Bessel type low pass filters are used. The cut-off frequencies of the filters are set to 2.5 kHz for both MSC and GSC. However, the order (up to 8th order), the type (Bessel and Butterworth) and the cut-off frequencies of the low pass filters can be modified through the device mask (device data input function). The measuring filter parameters may have significant impact on WT behavior in some phenomenon such as subsynchronous control interaction [12].

The MSC and GSC overcurrent protections use the root mean square (rms) values of the current values. When the current at any phase exceeds the used defined limit, it blocks the overloaded converter temporarily. The user defined converter pickup current and reset time are set to 2 pu and 50ms in the presented generic model.

The low voltage and overvoltage relays use rms voltages on each phase at FSC WT ac terminals and send a trip signal to the FSC circuit breaker when any of the phase rms voltage violates the limits defined as a function of time by the user. The voltage-time characteristics of the low voltage and overvoltage relays are set based on the technical requirements of Hydro-Quebec for the integration of wind generation [36].

The reader should refer to [16] for the modeling, implementation and utilization details of the generic model presented in this paper.

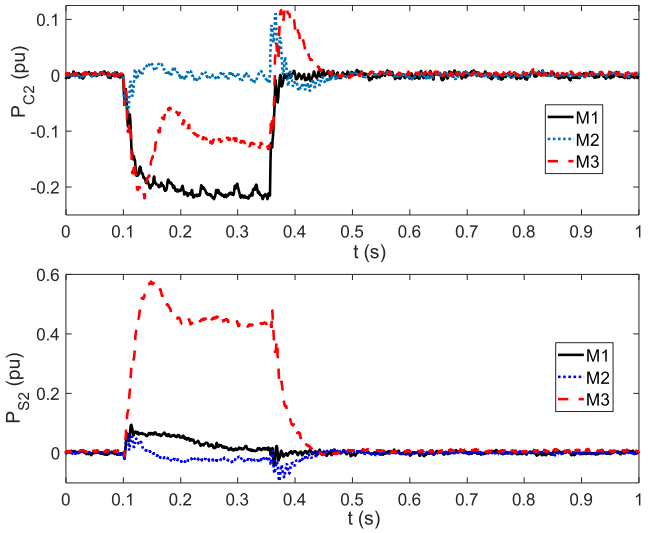

FIGURE 16. P_{C2} and P_{S2} of aggregated FSC WT in M1, M2 and M3.

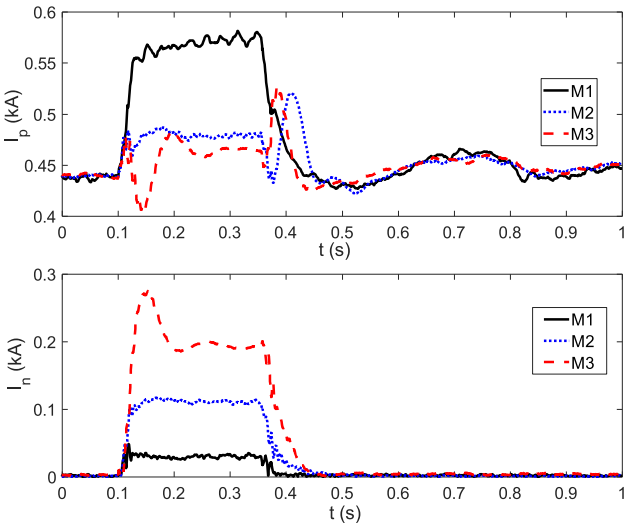

FIGURE 18. I_p and I_n of WP in M1, M2 and M3.

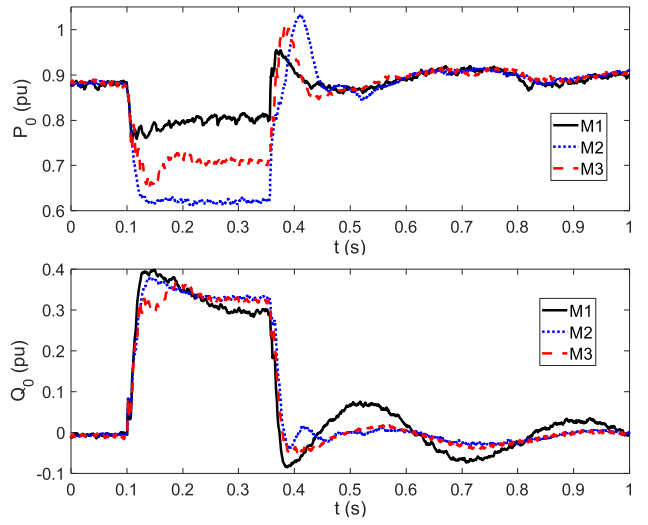

FIGURE 17. P_0 and Q_0 of aggregated FSC WT in M1, M2 and M3.

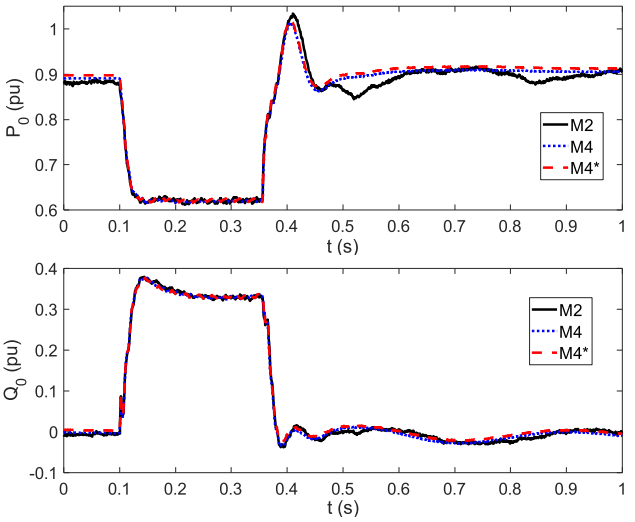

FIGURE 19. P_0 and Q_0 of aggregated FSC WT in M2 and M4.

VI. SIMULATIONS

The single-line diagram of the 120 kV, 60 Hz test system is shown in Fig. 15. The WP includes 45 WTs rated at 1.5 MW. The WP is operating at full load (under nominal wind speed) and under Q-control function of WPC with $Q'_{POI} = 0$. The reader should refer to [16], [29], [37] for wind park and 120 kV test system details.

Several simulations are performed for different fault types and locations using the simulation models (M1 to M4) presented in Table 1. However, only the 250 ms double line to ground (DLG) fault at BUS4 scenario is presented below due to space limitations. A long duration fault is applied for testing purpose. The simulation time-step is 10 μs (a typical value in DM usage) and total simulation time is 2 seconds.

As shown in Fig. 16, the simulated unbalanced fault results into second harmonic pulsations in the active power output of M1. These second harmonic pulsations (P_{C2}, P_{S2}) are eliminated in M2 at the expense of a reduction in the active power output of FSC WT (P_0), as seen in Fig. 17. M3 achieves injection of desired negative sequence reactive current at the expense of a reduction in in the active power output of FSC WT (see Fig. 17) and an increase in second harmonic oscillations in the GSC active power output (Fig. 16). On the other hand, the reactive power output of the FSC WT is similar in M1, M2 and M3. This is due to the same FRT requirement on positive sequence reactive currents.

The performance of M2 and M3 is limited to GSC rating. The DSC objectives cannot be achieved in both M2 and M3 when the required GSC current output exceeds its rating. It should be noted that, when the electrical distance between the WP and unbalanced fault decreases, larger GSC currents are required to achieve the DSC objectives in both M2 and M3.

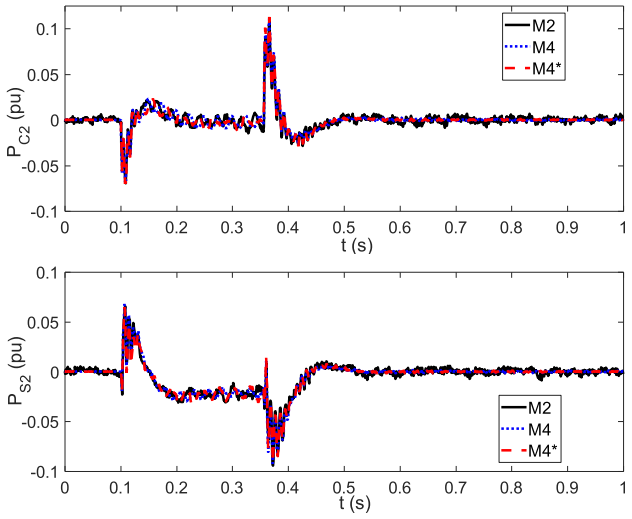

FIGURE 20. P_{C2} and P_{S2} of aggregated FSC WT in M2 and M4.

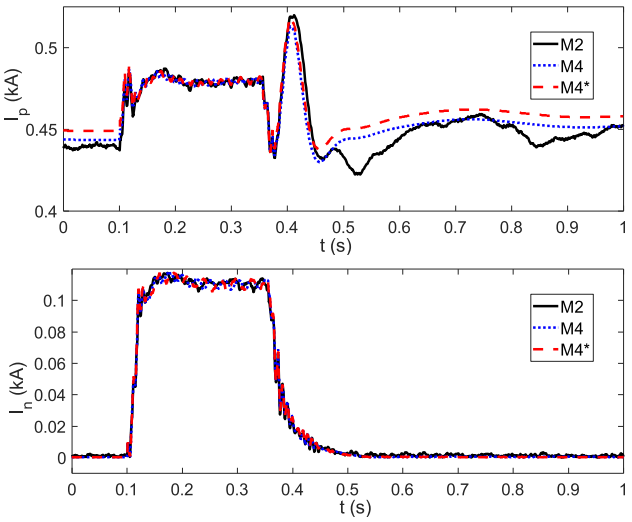

FIGURE 21. I_p and I_n of WP in M2 and M4.

TABLE 2. CPU timings (Intel i7-4900MQ CPU @ 2.8 GHz).

Model	M2	M4	M4*
CPU Time	144.7 s	99.5 s	28.8 s

The negative and positive sequence fault currents (I_n and I_p) of the WP in M1, M2 and M3 are illustrated in Fig. 18. The small negative sequence current injection in M1 is due to phase shift in low pass measuring filters [14]. M2 injects a considerable amount of negative sequence current to achieve mitigation of second harmonic power oscillations, but still quite low compared to M3. It should be noted that, this difference strongly depends on the unbalanced fault type, its electrical distance to the WP and GSC rating. It becomes less noticeable especially for the electrical distant faults such as an unbalanced fault at BUS6.

As shown in Fig. 19 - Fig. 21, AVM usage instead of DM provides acceptable accuracy even for 50 μs time step usage while providing a significant computational gain as illustrated in Table 2. M4$*$ in Fig. 19 - Fig. 21 is the M4 solution with 50 μs time step. In this simulation, the computational gain over DM is more than 5 when AVM is used with 50 μs time step. However, a higher computational gain can be expected while simulating a large scale power system.

VII. CONCLUSION

This paper presented a generic EMT model for FSC WT based WPs that can be used for wide range of WP integration studies. The considered topology uses a PMSG and ac-dc-ac converter system consisting two PWM VSCs. Although the collector grid and the FSC WTs are represented with their aggregated models, the overall control structure of the WP is preserved. The FSC WT and the WP control systems include the non-linearities, and the necessary transient and protection functions to simulate the accurate transient behavior of the WP.

The presented generic EMT model offers two DSC schemes (DSC1 and DSC2) in addition to the traditional CSC. The objective in DSC1 is mitigation of second harmonic pulsations in the active power output of FSC WT during unbalanced operating conditions or faults, while achieving the FRT requirement on positive sequence reactive currents. The objective in DSC2 is to reduce the negative sequence voltage by consuming negative sequence reactive power. DSC2 is implemented considering the recent VDE-AR-N 4120 Technical Connection Rules which has a negative sequence reactive current requirement in addition to the positive.

When GSC is operating under DSC1 instead of CSC, it produces much larger negative sequence currents (depending on fault location) to achieve the elimination (or reduction) of the second harmonic pulsations in the active power output of FSC WT. As the GSC outputs similar positive sequence reactive currents in both control schemes due to the strict FRT requirement, the GSC operating under decoupled sequence control outputs also less positive sequence active currents due to strict GSC current output limit. This results into higher negative sequence and lower positive sequence currents during unbalanced faults that are especially electrically close to the point of interconnection. Hence, the GSC control scheme is expected to have significant positive impact on power system protection performance by reducing the misoperation possibility. The reduced GSC positive sequence active current output also results into less power injection to the grid during fault. This may have an impact on transient stability margin of the power system.

When GSC is operating under DSC2, the negative sequence current injection is much larger compared the DSC1. Hence, it can reduce the possibility of protection system misoperation further. However, the desired negative sequence current injection is achieved at the expense of very large second harmonic pulsations in active power output.

The presented generic EMT model also offers two converter modeling options: detailed model (DM) and average value model (AVM). Simulation results demonstrated that,

AVM usage instead of DM provides acceptable accuracy even for larger simulation time steps. AVM eliminates computational inefficiencies of DM and provides very high computational performance.

REFERENCES

[1] S. V. Bozhko, R. Blasco-Giménez, R. Li, J. C. Clare, and G. M. Asher, "Control of offshore DFIG-based wind farm grid with line-commutated HVDC connection," *IEEE Trans. Energy Convers.*, vol. 22, no. 1, pp. 71–78, Mar. 2007.

[2] I. Erlich, J. Kretschmann, J. Fortmann, S. Mueller-Engelhardt, and H. Wrede, "Modeling of wind turbines based on doubly-fed induction generators for power system stability studies," *IEEE Trans. Power Syst.*, vol. 22, no. 3, pp. 909–919, Aug. 2007.

[3] J. Fortmann, S. Engelhardt, J. Kretschmann, C. Feltes, and I. Erlich, "New generic model of DFG-based wind turbines for RMS-type simulation," *IEEE Trans. Energy Convers.*, vol. 29, no. 1, pp. 110–118, Mar. 2014.

[4] *WECC Wind Power Plant Dynamic Modeling Guide, Prepared by: WECC Renewable Energy Modeling Task Force*, Western Electr. Coordinating Council Model. Validation Work Group, Salt Lake City, UT, USA, Apr. 2014.

[5] J. J. Sanchez-Gasca, "Generic wind turbine generator models for WECC—A second status report," in *Proc. IEEE Power Energy Soc. Gen. Meeting*, Denver, CO, USA, Jul. 2015, pp. 1–5.

[6] P. Pourbeik *et al.*, "Generic dynamic models for modeling wind power plants and other renewable technologies in large-scale power system studies," *IEEE Trans. Energy Convers.*, vol. 32, no. 3, pp. 1108–1116, Sep. 2016.

[7] L. Lindgren, J. Svensson, and L. Gertmar, "Generic models for wind power plants—Needs and previous work," Elforsk, Lund Univ., Lund, Sweden, Tech. Rep., Jul. 2012.

[8] J. M. Garcia, "Voltage control in wind power plants with doubly fed generators," Ph.D. dissertation, Dept. Elect. Eng., Aalborg Univ., Aalborg, Denmark, Sep. 2010.

[9] D. N. Hussein, M. Matar, and R. Iravani, "A type-4 wind power plant equivalent model for the analysis of electromagnetic transients in power systems," *IEEE Trans. Power Syst.*, vol. 28, no. 3, pp. 3096–3104, Aug. 2013.

[10] D. N. Hussein, M. Matar, and R. Iravani, "A wideband equivalent model of type-3 wind power plants for EMT studies," *IEEE Trans. Power Del.*, vol. 31, no. 5, pp. 2322–2331, Oct. 2016.

[11] O. Göksu, M. Altin, J. Fortmann, and P. E. Sørensen, "Field validation of IEC 61400-27-1 wind generation type 3 model with plant power factor controller," *IEEE Trans. Energy Convers.*, vol. 31, no. 3, pp. 1170–1178, Sep. 2016.

[12] U. Karaagac, J. Mahseredjian, S. Jensen, R. Gagnon, M. Fecteau, and I. Kocar, "Safe operation of DFIG-based wind parks in series-compensated systems," *IEEE Trans. Power Del.*, vol. 33, no. 2, pp. 709–718, Apr. 2018.

[13] M. Ghafouri, U. Karaagac, H. Karimi, S. Jensen, J. Mahseredjian, and S. O. Faried, "An LQR controller for damping of subsynchronous interaction in DFIG-based wind farms," *IEEE Trans. Power Syst.*, vol. 32, no. 6, pp. 4934–4942, Nov. 2017.

[14] A. Haddadi, I. Kocar, U. Karaagac, J. Mahseredjian, and E. Farantatos, "Impact of renewables on system protection: Wind/PV short-circuit phasor model library and guidelines for system protection studies," EPRI, Palo Alto, CA, USA, Tech. Rep. 3002008367, 2016.

[15] R. Teodorescu, M. Liserre, and P. Rodriguez, *Grid Converters for Photovoltaic and Wind Power Systems*. Hoboken, NJ, USA: Wiley, 2011.

[16] U. Karaagac, J. Mahseredjian, H. Gras, H. Saad, J. Peralta, and L. D. Bellomo, "Simulation models for wind parks with variable speed wind turbines in EMTP-RV," Polytechnique Montréal, Montreal, QC, Canada, Res. Rep., Mar. 2017.

[17] I. Erlich, T. Neumann, F. Shewaega, P. Schegner, and J. Meyer, "Wind turbine negative sequence current control and its effect on power system protection," in *Proc. IEEE Power Energy Soc. Gen. Meeting*, Vancouver, BC, Canada, Jul. 2013, pp. 1–5.

[18] M. Nagpal and C. Henville, "Impact of power-electronic sources on transmission line ground fault protection," *IEEE Trans. Power Del.*, vol. 33, no. 1, pp. 62–70, Feb. 2018.

[19] *Impact of Inverter Based Generation on Bulk Power System Dynamics and Short-Circuit Performance, PES-TR68, IEEE/NERC Task Force on Short-Circuit and System Performance Impact of Inverter Based Generation*, Jul. 2018.

[20] *Technische Regeln den Anschluss von Kundenanlagen an das Hochspannungsnetz und Deren Betrieb (TAR Hochspannung), VDE-AR-N 4120 Anwendungsregel*, Oct. 2018.

[21] O. Anaya-Lara, N. Jenkins, J. Ekanayake, P. Cartwright, and M. Hughes, *Wind Energy Generation: Modelling and Control*. Hoboken, NJ, USA: Wiley, 2009.

[22] N. W. Miller, W. W. Price, and J. J. Sanchez-Gasca, "Dynamic modeling of GE 1.5 and 3.6 wind turbine-generators," GE-Power Syst. Energy Consulting, Gen. Electr. Int., Schenectady, NY, USA, Tech. Rep., Oct. 2003.

[23] *Wind Turbines—Part 27-1: Electrical Simulation Models—Wind Turbines*, IEC Standard 61400-27-1, 2015.

[24] G. Abad, J. López, M. Rodríguez, L. Marroyo, and G. Iwanski, *Doubly Fed Induction Machine: Modeling and Control for Wind Energy Generation*. Hoboken, NJ, USA: Wiley, 2011.

[25] M. Singh and S. Santoso, "Dynamic models for wind turbines and wind power plants," Univ. Texas Austin, Nat. Renew. Energy, Austin, TX, USA, Tech. Rep., Oct. 2011.

[26] V. Akhmatov, A. H. Nielsen, J. K. Pedersen, and O. Nymann, "Variable-speed wind turbines with multi-pole synchronous permanent magnet generators. Part I: Modelling in dynamic simulation tools," *Wind Eng.*, vol. 27, no. 6, pp. 531–548, Dec. 2003.

[27] L. Harnefors and H. P. Nee, "Model-based current control of ac machines using the internal model control," *IEEE Trans. Ind. Appl.*, vol. 34, no. 1, pp. 133–141, Jan./Feb. 1998.

[28] *Grid Code—High and Extra High Voltage*, E.ON Netz GmbH, Bayreuth, Germany, Apr. 2006.

[29] "Impact of renewables on system protection: Short-circuit phasor models of renewables and impact of renewables on power swing detection and distance protection," EPRI, Palo Alto, CA, USA, Tech. Rep. 3002005765, 2016.

[30] P. Rodriguez, J. Pou, J. Bergas, J. I. Candela, R. P. Burgos, and D. Boroyevich, "Decoupled double synchronous reference frame PLL for power converters control," *IEEE Trans. Power Electron.*, vol. 22, no. 2, pp. 584–592, Mar. 2007.

[31] J. Mahseredjian, S. Dennetière, L. Dubé, B. Khodabakhchian, and L. Gérin-Lajoie:, "On a new approach for the simulation of transients in power systems," *Electr. Power Syst. Res.*, vol. 77, no. 11, pp. 1514–1520, Sep. 2007.

[32] S. R. Sanders, J. M. Noworolski, X. Z. Liu, and G. C. Verghese, "Generalized averaging method for power conversion circuits," *IEEE Trans. Power Electron.*, vol. 6, no. 2, pp. 251–259, Apr. 1991.

[33] J. Morren, S. W. H. de Haan, P. Bauer, J. Pierik, and J. Bozelie, "Comparison of complete and reduced models of a wind turbine with doubly-fed induction generator," in *Proc. 10th Eur. Conf. Power Electron. Appl.*, Toulouse, France, Sep. 2003, pp. 1D–10D.

[34] J. G. Slootweg, H. Polinder, and W. L. Kling, "Representing wind turbine electrical generating systems in fundamental frequency simulations," *IEEE Trans. Energy Convers.*, vol. 18, no. 4, pp. 516–524, Dec. 2003.

[35] J. Peralta, H. Saad, U. Karaagac, J. Mahseredjian, S. Dennetièe, and X. Legrand, "Dynamic modeling of MMC-based MTDC systems for the integration of offshore wind generation," in *Proc. CIGRE Canada Conf. Power Syst.*, Montreal, QC, Canada, Sep. 2012, pp. 1–12.

[36] *Transmission Provider Technical Requirements for the Connection of Power Plants to the Hydro-Quebec Transmission System*, Hydro Quebec Transenergie, Montreal, QC, Canada, 2009.

[37] T. Kauffmann, U. Karaagac, I. Kocar, S. Jensen, J. Mahseredjian, and E. Farantatos, "An accurate type III wind turbine generator short circuit model for protection applications," *IEEE Trans. Power Del.*, vol. 32, no. 6, pp. 2370–2379, Dec. 2017.